Polyphase-Coded FM (PCFM) Radar Waveforms, Part I: Implementation

[1]Shannon D. Blunt, *IEEE Senior Member,* [2]Matthew Cook, *IEEE Member,*
[1]John Jakabosky, *IEEE Student Member,* [3]Jean de Graaf, *IEEE Member*,
and [4]Erik Perrins, *IEEE Senior Member*

[1]S.D. Blunt and J. Jakabosky are with the Electrical Engineering & Computer Science Dept., Radar Systems & Remote Sensing Lab, of the University of Kansas, Lawrence, KS.

[2]M. Cook is with the University of Kansas and Garmin International in Olathe, KS.

[3]J. de Graaf is with the Radar Division of the US Naval Research Laboratory, Washington, DC.

[4]E. Perrins is with the Electrical Engineering & Computer Science Dept., Communications & Signal Processing Lab, of the University of Kansas, Lawrence, KS.

Abstract

Polyphase radar codes promise enhanced performance and flexibility due to greater design freedom. While the search for better codes continues, the implementation issues of transmitter bandlimiting and nonlinear distortion have precluded their widespread use in high-power systems. This paper introduces a modified continuous phase modulation (CPM) implementation that converts an arbitrary polyphase code into a nonlinear FM waveform that is constant envelope and spectrally well-contained. Experimental results assess the receive sampling and pulse compression effects.

Keywords
Radar, pulse compression, nonlinear distortion, continuous phase modulation, radio spectrum management

I. INTRODUCTION

The notion of phase coding for the purpose of radar pulse compression has been around for several decades with an extensive litany of contributions such as Barker codes [2], P-codes [3,4], minimum peak sidelobe (MPS) codes [5], and many others (see [6, Chap. 6] for a thorough survey). The metric of goodness for a code is generally based upon some measure of the time (range) sidelobes provided by the code's autocorrelation, with factors such as Doppler tolerance and "thumbtack" characteristics as additional considerations. The size of the phase constellation for a code (the number of possible phase states) can theoretically be as small as 2 for binary codes up to an infinitude of values distributed over the 2π phase continuum. Since phase coding was first conceived, there has been an ongoing effort to discover ever longer codes with lower autocorrelation sidelobes (recently, for example [7,8]). The explosive growth in waveform diversity research has also expanded code search efforts to encompass new paradigms such as MIMO ([9] and references therein) and adaptive waveform design ([10] and references

therein). Fundamentally, all these efforts, for varying sensing modes and constraints, seek to optimize the means with which the active sensor queries the environment.

While this intense effort has focused on the design of various coding schemes, far less emphasis has been placed on their physical implementation. Consider the mathematical representation of a continuous, baseband code that consists of a set of contiguous, constant amplitude, rectangular chips (or sub-pulses) that are modulated by the phase values of the code (Figure 1). This idealized representation is the mathematical model used by virtually all code search strategies seeking to determine an optimal sequence of code phase values [11]. However, as Levanon and Mozeson elaborate [6, pp. 145-155], the instantaneous phase change between consecutive chips of the code results in extended spectral sidelobes having a $\sin(x)/x$ envelope. An operational transmitter, which includes driver amplifiers and an exciter, will not pass these extended spectral sidelobes due to inherent bandlimiting. Thus the transmitter, which possesses nonlinear characteristics as well, emits a physical signal that is a distorted version of the idealized continuous model of the code. Generally speaking, the nature of this distortion induces range straddling (or cusping) losses on receive [12] due to the bandlimiting distortion and spectral regrowth due to intermodulation products that are a nonlinear result of operating the power amplifier (PA) in saturation [13]. Of course, PA saturation is necessary to achieve the high efficiency required for high-power systems.
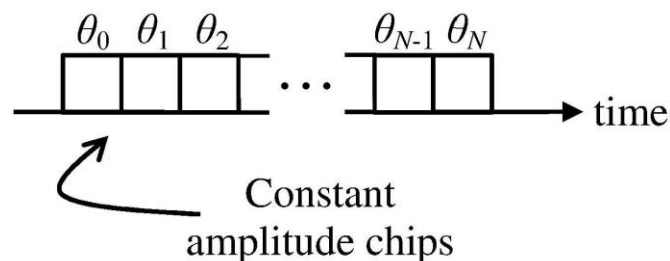

Figure 1: Idealistic representation of a polyphase-coded waveform

For the reasons stated above and because there tends to be a general looseness to the vernacular in the literature, it is useful to clarify distinctly the terms *code*, *waveform*, and *emission* as they are applied here. The *code* is a mathematical abstraction consisting of a finite set of sequential phase values $[\theta_0, \cdots, \theta_N]$. The code elements are typically represented as corresponding to rectangular chips, though as discussed above this idealistic structure is not physically realizable without distortion. In contrast, the *waveform* is the continuous temporal signal that is modulated onto a pulse. Perhaps the most well-known waveform is the linear frequency modulated (LFM) chirp [6, pp. 57-61]. The purpose of the implementation proposed here is to effect the conversion of a discrete code into a continuous waveform that is amenable to the bandlimiting/nonlinear characteristics of the transmitter. Finally, we shall refer to the signal that the radar physically launches into the environment as the *emission*, which in reality is a distorted version of the waveform due to transmitter effects. This definition also includes the pulse envelope, as the non-instantaneous rise and fall times likewise influence the nature of the emission, and electromagnetic effects from the antenna and potentially the radar platform. Enabled by the continuous phase modulation (CPM) implementation scheme developed here, optimization of the physical emission is subsequently addressed in the companion paper [14].

It is well known that a waveform should have a constant envelope to avoid some of the nonlinear distortion imparted to amplitude modulation (AM) in the saturated PA as well as to maximize power-added efficiency (PAE) and maintain "energy on target" for detection sensitivity. It tends to be less appreciated, however, that a waveform must also be continuous, and thus differentiable, with sufficient bandlimiting to minimize the

spectral shaping imposed by the transmitter that can produce additional AM effects leading into the PA, subsequently compounding distortion. For this reason, combined with the fact that a suitable implementation had not been developed, the use of arbitrary polyphase codes has previously been of limited use for high-power radar applications.

For the subset of polyphase codes that possess only two antipodal phase states (binary codes), there are existing techniques to convert the code into a constant envelope, continuous waveform that can be transmitted with minimal distortion. The two most common techniques are derivative phase shift keying (DPSK) [15] and the biphase-to-quadriphase (BTQ) transformation [16], which is a form of minimum shift keying (MSK). Of the two, the latter is superior from a spectral containment standpoint [15], though both are fundamentally limited in terms of range sidelobe performance due to the constraint of binary phase which limits the design degrees of freedom.

Another approach that has been investigated to constrain the spectrum of coded waveforms is to replace the rectangular chips with windowed (and thereby truncated) sinc kernel functions [15,17]. While this approach has been shown to achieve very good spectral containment, which is of growing importance due to increasing congestion of the RF spectrum [18], the sinc kernel also produces amplitude modulation that subsequently requires linear amplification. To generate these waveforms with nonlinear amplification (higher PAE), a configuration comprising dual nonlinear amplifiers followed by a summer, otherwise known as LINC (LInear amplification with Nonlinear Components) [13], has been suggested. It has been experimentally demonstrated that high transmit power may still conceivably be achieved for this type of configuration as long as adequate cross-calibration of the two amplifiers in the LINC can be maintained. Of

course, the lost "energy on target" from AM effects still translates into reduced receive SNR, and thus lost sensitivity.

To address the lack of a suitable implementation for arbitrary polyphase codes, a modified version of the continuous phase modulation (CPM) framework [19] is presented here. Being spectrally well-contained (continuous), power efficient (constant envelope), and easy to implement using standard FM [19, Chap. 6], CPM is currently used for the demanding applications of aeronautical telemetry [20,21] and deep-space communication [22], as well as within the Bluetooth wireless standard [23] to maximize battery life. For the application to radar, it is necessary to modify the form of CPM used in communications so that the properties of optimized polyphase codes can be maintained to the degree possible. It is shown via experimental measurements that the resulting polyphase-coded FM (PCFM) waveforms exhibit effective spectral containment, which translates into reduced transmitter distortion and straddling losses relative both to the idealized implementation and to a near-idealistic variant to "slow down" the phase transitions.

The remainder of the paper is organized as follows. Section II presents the traditional CPM implementation used for communications and then introduces the new formulation for the implementation of PCFM radar waveforms. In Section III the receiver implications of employing PCFM waveforms are discussed. Finally, in Section IV experimental results demonstrate the efficacy of this new CPM implementation using a LFM-derived polyphase code for benchmarking and a previously optimized code to demonstrate the new waveform generation capability as well as highlight where further performance improvement may be obtained.

II. CONTINUOUS PHASE MODULATION (CPM)

For communications the CPM implementation provides a spectrally efficient (in bits/Hz) and power efficient means with which to modulate a stream of digitally encoded information. For this purpose, there are different variations of CPM that depend on the spectral requirements of the physical emission and the computational complexity for the communication receiver [19]. In general, the CPM implementation for communications can be expressed mathematically via the scheme depicted in Fig. 2. Here a stream of information-bearing data symbols α_i is multiplied by a modulation index h_i, and then this modified stream is modulated onto an impulse train. The sequence of weighted impulses $p(t;\underline{\alpha})$ is convolved with the frequency shaping filter $g(t)$ and is subsequently integrated to produce a continuous signal. Following scaling by 2π, the resulting phase-domain signal $\phi(t;\underline{\alpha})$ is converted into the complex baseband signal $s(t;\underline{\alpha})$ for modulation onto the carrier.
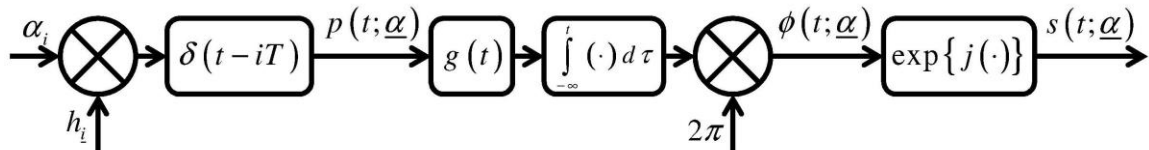

Figure 2: Generic CPM implementation for communications

As an example, Fig. 3 illustrates the "phase cylinder" of the PCM/FM version of CPM [19] where it is observed that, unlike the idealistic polyphase radar coding scheme of Fig. 1 in which the phase is constant over a chip interval, the CPM phase is always in transition. It is this state of continuous transition that enables CPM to provide such good spectral containment in comparison to other modulation schemes [19].
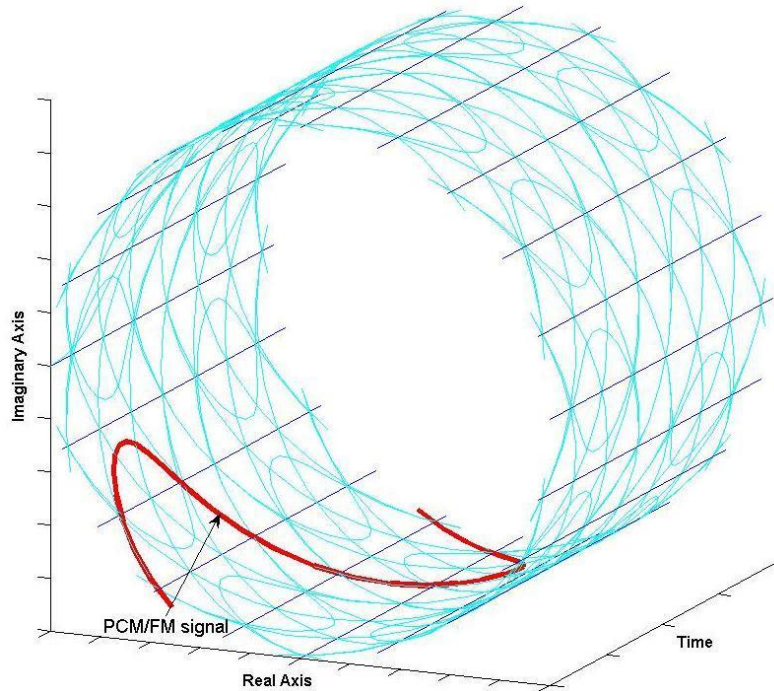
Figure 3: CPM "phase cylinder" for the PCM/FM communication signal [19]

For the communication implementation in Fig. 2 there is a requirement to preserve the encoded information such that it can be recovered at a receiver while the physical structure of the "waveform" is only important to the degree that it impacts spectral content and receiver performance. In contrast, a radar waveform carries no information, yet its modulation structure is vitally important to ensure the required range resolution and sensitivity following receiver pulse compression, whereby information on the illuminated environment is extracted. For radar, the CPM implementation can thus be simplified to eliminate aspects associated with information-bearing signals and must also be modified to preserve the desirable properties of optimized polyphase codes.

A new form of CPM implementation is proposed that is appropriate for polyphase radar codes (Fig. 4), where a train of N consecutive impulses with time separation T_p are formed such that the total pulsewidth is $T = NT_p$. The nth impulse is weighted by

α_n, which is the phase change between successive chips of the polyphase code as determined by

$$\alpha_n = \Psi(\tilde{\alpha}_n) = \begin{cases} \tilde{\alpha}_n & \text{if } |\tilde{\alpha}_n| \leq \pi \\ \tilde{\alpha}_n - 2\pi \operatorname{sgn}(\tilde{\alpha}_n) & \text{if } |\tilde{\alpha}_n| > \pi \end{cases}, \tag{1}$$

where

$$\tilde{\alpha}_n = \theta_n - \theta_{n-1} \quad \text{for} \quad n = 1, \cdots, N, \tag{2}$$

$\operatorname{sgn}(\bullet)$ is the signum operation, and θ_n is the phase value of the nth chip in the length $N+1$ polyphase code. The shaping filter $g(t)$ is essentially the same as that used for communications where the most common examples are rectangular (RECT) and raised cosine (RC). The requirements on $g(t)$ are: 1) that it integrates to unity over the real line; and 2) that it has time support on $[0, T_p]$, which is specific to radar so that the chip intervals do not overlap in time. The integration stage in Fig. 4 is initialized to θ_0 and the sequence of phase changes are collected into the vector $\mathbf{x} = [\alpha_1 \ \alpha_2 \ \cdots \ \alpha_N]^T$, which parameterizes the complex baseband PCFM waveform

$$s(t; \mathbf{x}) = \exp\left\{ j \left(\int_0^t g(\tau) * \left[\sum_{n=1}^N \alpha_n \delta\big(\tau - (n-1)T_p\big) \right] d\tau + \theta_0 \right) \right\}. \tag{3}$$

The benefit of enabling the practical implementation of existing optimized codes is clear. Furthermore, the transmitter hardware requirements for this new version of CPM are the same as previous versions [19, Chap. 6] that rely on standard FM (that is, it does not require an arbitrary waveform generator). However, as shown in the companion paper [14], the real potential of this implementation is the linkage it provides between the emission from the physical transmitter (complete with spectral shaping and nonlinear characteristics) and the optimization of the underlying polyphase code. It is also

interesting to note that, if a rectangular shaping filter is selected for $g(t)$, the phase of the resulting PCFM waveform could be viewed as a form of first-order hold as compared to the zero-order hold phase representation of the idealist phase code from Fig. 1.
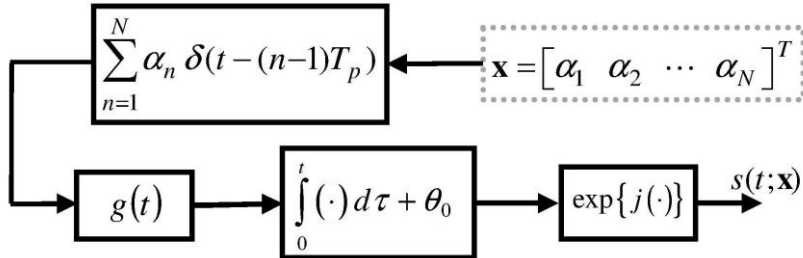

Figure 4: Proposed CPM implementation to generate polyphase-coded FM (PCFM) waveforms

III. RECEIVE FILTERING FOR PCFM RADAR WAVEFORMS

Because pulsed radar emissions have a finite time support given by the pulsewidth *T*, it is not possible to realize perfect bandlimiting. As such, receive sampling involves a trade-off between adequate fidelity, which is improved by increasing the sampling rate, and computational cost and noise rejection, which are improved by lowering the sampling rate. The degree of spectral containment of the radar waveform plays an important role in determining this trade-off.

We can define the receive sampling period as

$$T_S = \frac{T}{K(N+1)} \; , \tag{4}$$

where $N+1$ is the number of chips in the underlying code and K is the number of samples per chip interval. Thus the *chip width* is $T_c = T/(N+1) = KT_s$. Note that, in contrast, a PCFM waveform (via Fig. 4) is driven by a sequence of N phase changes and is thus constructed from N weighted impulses having a time separation of $T_p = T/N$. However, we shall use the sampling definition from (4) to provide a convenient

framework with which to compare performance across different implementations. Based on (4), the sampled version of a continuous waveform $s(t)$ will possess $K(N+1) \doteq \tilde{N}$ samples over the pulsewidth T. By using this formulation, the receiver fidelity in terms of sampling rate can be assessed as a function of K.

The first-null (mainlobe) bandwidth of an idealistic polyphase-coded waveform (Fig. 1) is $B_{\text{null}} = 1/T_C$ [6, Sect. 6.8]. On neglecting small values of N, one observes that $T_c \approx T_p$ such that PCFM waveforms yield essentially the same mainlobe bandwidth. Of course, outside the mainlobe it is known that idealistic coded waveforms exhibit a rather slow spectral roll-off of 6 dB/octave, thereby producing a "spectral skirt" [6, Sect. 6.8], an attribute that is largely absent for PCFM waveforms as demonstrated in Section IV.

Denoting $y(n)$ and $h(n)$ as the discrete-time baseband sequences for the sampled received signal and the receiver matched filter, respectively, the straddling loss [12, 24] at each delay offset τ on the interval $[0, T_s]$ can be defined as the metric

$$\text{Straddling Loss}\,(\tau) \;=\; -10\log\left\{\max_n \left| h(n) * y(n+\tau) \right|^2\right\}, \tag{5}$$

with $y(n+\tau)$ representing the response from a point scatterer with delay offset τ and where $y(n+\tau)$ and $h(n)$ are scaled to have unit length (so that a 0 dB result signifies no loss due to a perfect match). The interval $[0, T_s]$ represents the possible delay of the echo relative to the timing of the receive samples that are obtained at the rate of $1/T_s$. By using the metric in (5), the "goodness" of different waveform implementations and their associated (presumed) matched filter can be evaluated.

The structure of polyphase codes (finite number of chips having arbitrary phase) makes them convenient to optimize via various search strategies [14]. However, retaining

this optimality requires that: *a*) the nature of the code-to-waveform implementation ensures that the subsequent emission is minimally affected by the transfer function of the transmitter, which can vary depending on such factors as memory effects, impedance mismatch, and temperature; and/or *b*) the code optimization actually accounts for the waveform implementation and transmitter distortion. Regarding the former, it is shown in Sect. IV that PCFM waveforms incur less distortion from the transmitter than idealistic coded waveforms. This issue of waveform/emission fidelity impacts the performance of the receiver filter via mismatch loss (assuming use of the matched filter) and the degree to which the optimized range sidelobe level is preserved. The latter is the subject of the companion paper [14].

Use the least squares (LS) pulse compression formulation from [25] within the waveform sampling context above to form the $((M+1)\tilde{N}-1) \times M\tilde{N}$ matrix

$$
\mathbf{A} = \begin{bmatrix}
s_1 & 0 & \cdots & 0 \\
\vdots & s_1 & & \vdots \\
s_{\tilde{N}} & \vdots & \ddots & 0 \\
0 & s_{\tilde{N}} & & s_1 \\
\vdots & & \ddots & \vdots \\
0 & \cdots & 0 & s_{\tilde{N}}
\end{bmatrix},
\tag{6}
$$

where $M\tilde{N}$ is to be the length of a mismatch filter (with M typically on the order of 2 to 4) and the length-$\tilde{N}$ column vector $\mathbf{s}$ is the sampled version of $s(t;\mathbf{x})$ from (3). Each column of $\mathbf{A}$ is completed by inserting a total of $M\tilde{N}-1$ zeroes above and below $\mathbf{s}$ as appropriate. Based on [25], the LS mismatch filter (MMF) is readily found to be

$$
\mathbf{h} = \left(\mathbf{A}^H \mathbf{A}\right)^{-1} \mathbf{A}^H \mathbf{e}_m
\tag{7}
$$

where $(\bullet)^H$ denotes the complex conjugate transpose operation and $\mathbf{e}_m$ is the length

$(M+1)\tilde{N}-1$ elementary vector with a 1 in the mth element and zero elsewhere. The

value of m is normally in the neighborhood of $((M+1)\tilde{N}-1)/2$.

Because $\mathbf{s}$ is "over-sampled" by the factor K, the matrix $\left(\mathbf{A}^H\mathbf{A}\right)$ can become ill-

conditioned for $K>1$ depending on the degree of spectral containment of the emission.

A well-known solution to such a problem is diagonal loading as

$$\mathbf{h}=\left(\tilde{\mathbf{A}}^H\tilde{\mathbf{A}}+\delta\mathbf{I}\right)^{-1}\tilde{\mathbf{A}}^H\mathbf{e}_m, \tag{8}$$

where δ is the loading factor and $\mathbf{I}$ is the $M\tilde{N}\times M\tilde{N}$ identity matrix. The particular

value for δ depends on the trade-off between range sidelobes and mismatch loss [26].

In (8), $\mathbf{A}$ has also been replaced with $\tilde{\mathbf{A}}$. As discussed in [26], the formulation in

(7) can produce a range super-resolution effect at the cost of higher range sidelobes. A

simple "beam spoiling" approach to trade range resolution for reduced range sidelobes

within the LS MMF context [27] is to replace the rows of $\mathbf{A}$ surrounding the mth row

with zeros. Thus the matrix $\tilde{\mathbf{A}}$ is obtained by setting the elements of the $\lceil K/2\rceil$ rows

above and the $\lceil K/2\rceil$ rows below the mth row to zero so that the resulting range

resolution closely approximates the nominal resolution of the matched filter.

IV. Evaluation of PCFM Waveforms

To evaluate the efficacy of the new CPM implementation for polyphase radar codes,

two sets of waveforms are considered. The first set involves different implementations of

a code derived from the basic LFM waveform and is used in Sections IV.A through IV.D

to establish a performance baseline. The second set is used in Sect. IV.E to demonstrate

the capability of the CPM implementation to generate a physically realizable radar emission from an existing optimized code (here via a length-64 polyphase Barker code [28]).

For the first set, four different implementations of the P4 code [4] are considered (see Table 1), where each implementation generates a continuous waveform that is loaded onto an arbitrary waveform generator (AWG). This code is chosen because its implementation via CPM using the rectangular (RECT) shaping filter $g(t)$ yields a PCFM waveform that very closely approximates the well-known LFM chirp (with piecewise linear phase transitions) and thus serves as a standard benchmark for comparison. The four implementations considered include this version, denoted as PCFM-RECT, another version denoted as PCFM-RC that uses the raised-cosine shaping filter, an "Ideal Chip" version of the waveform that is based on rectangular chips with instantaneous transitions (or as nearly so as can be physically achieved), and a "10% Transition" version of the Ideal Chip waveform where each phase transition involves a linear interpolation in phase over a time interval that is 10% of each chip width. This final waveform represents a known ad hoc approach to remediate the extended spectrum of the idealistic waveform due to "instantaneous" phase switching [6, Sect. 6.8].

Table 1: Waveform implementation schemes and their characteristics

Implementation	Waveform Characteristics
Ideal Chip	Fastest phase transition possible given AWG limitations
10% Transition	Linearly interpolated phase transition over 10% of chip width
PCFM-RECT	Uses a rectangular filter for $g(t)$;
PCFM-RC	Uses a raised-cosine filter for $g(t)$

Each of the waveforms in Table 1 is generated in Matlab using a sampling rate of 150 samples / chip width and $N = 64$ chips. Each waveform is then loaded onto an AWG

that is used to drive an existing S-band test setup that includes a mixer, pre-amplifier, bandpass filter, and a class AB solid-state GaN power amplifier (PA). A loopback capture of the resulting PA output "emission" is down-converted to baseband, is analog lowpass filtered, and is then sampled at a rate commensurate with 150 samples / chip width to match the original waveform. In this manner, for each implementation there is an "AWG waveform" and a "loopback emission" that allow comparison of how each implementation is affected by transmitter spectral shaping and nonlinear distortion. While receiver-induced distortion may also be present in the loopback emission, it is expected to be negligible relative to the transmitter distortion due to the absence of receiver clipping.

The four implementations are evaluated in terms of pulse shape, spectral content, range straddling mismatch losses, and pulse compression filter response. The pulse shape is examined to demonstrate the deficiency of idealized coded waveforms and, in contrast, the practical benefit of CPM-implemented PCFM waveforms. The spectral content of the waveform, and by extension the physical emission from the transmitter, is used to illustrate the robustness of PCFM waveforms to transmitter distortion and the potential to improve spectral containment for high-power radar systems, particularly given the expectation of more stringent spectral requirements in the future (the current Radar Spectrum Engineering Criteria (RSEC) roll-off of 20 dB/decade may become 30 or 40 dB/decade [29]). Spectral content also determines the nature of the digital pulse compression filter in the receiver and the impact on range straddling losses.

A) Transmit Effects - Pulse Shape

The pulse shape of the loopback emission that results from driving each of the AWG-implemented waveforms from Table 1 into the transmitter provides an indication

of the impact the transmitter (without antenna effects) has upon each individual waveform. Figures 5 and 6 depicts the pulse shapes (full and zoom-in, respectively) of the loopback emissions that result for the four different implementations of the P4 code.
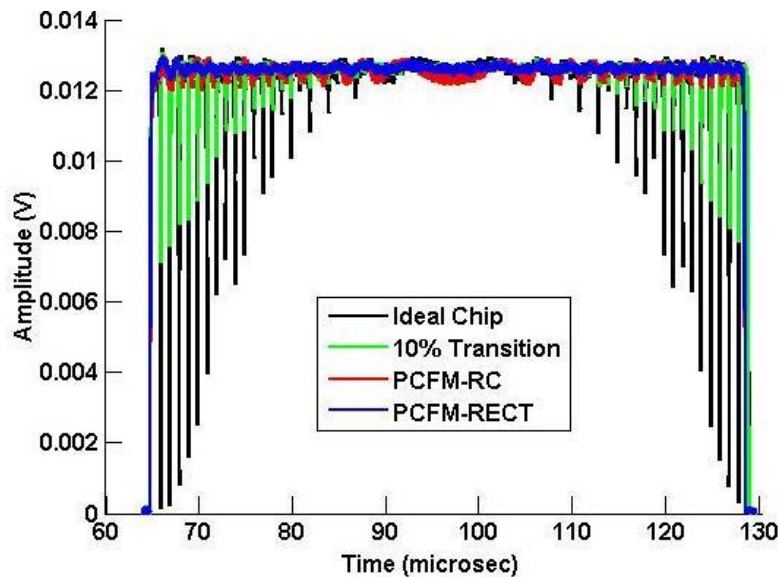

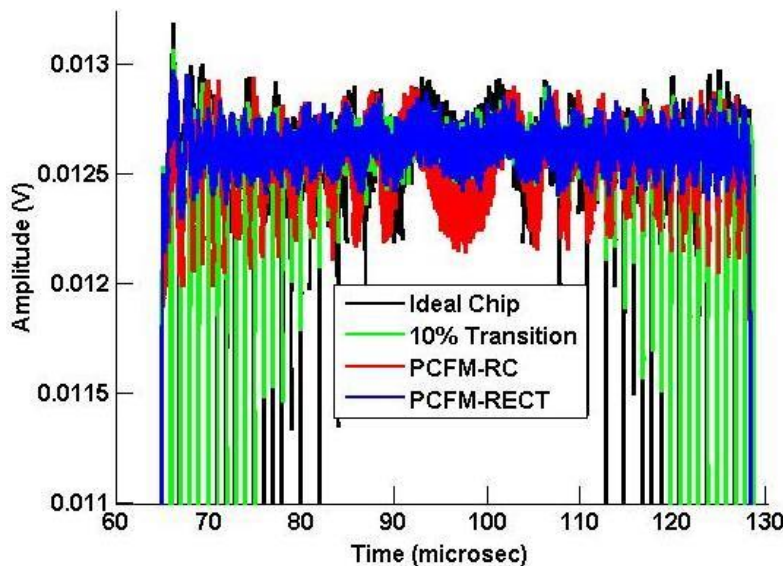**Figure 5: Pulse shapes for the four loopback emissions following transmitter distortion**

Figure 6: Pulse shapes for the four loopback emissions following transmitter distortion (zoom-in)

As expected the Ideal Chip version, and to a slightly lesser degree the 10% Transition version, induce nulls that coincide with chip transitions. This effect is well

known and arises from intrinsic bandlimiting in the transmitter. In contrast, the two PCFM emissions, particularly the PCFM-RECT version, realize only small amplitude ripples as a result of the transmitter nonlinearity that induces phase modulation (PM) to AM effects, which is common for power amplifiers.

B) Transmit Effects - Spectral Content

The cause of the chip transition nulls in Figs. 5 and 6 can be observed by comparing the spectral content of each implementation in terms of the AWG-implemented waveform and subsequent loopback emission (Figs. 7-10). In Figs. 7 and 8, the AWG waveforms for the Ideal Chip and 10% Transition versions clearly have significant spectral spreading, though the latter is somewhat reduced by the ad hoc incorporation of phase transitions. Due to this extended spectral content, the spectral shaping induced by the transmitter imposes a penalty in terms of distortion and, consequently, mismatch loss. In quantitative terms, the spectral content of the AWG waveform and loopback emissions begin deviating from one another in the vicinity of the first sidelobe (around −13 dB) for both of these cases. Also, the loopback emission for the 10% Transition case possesses a noise-limited bandwidth of roughly 25 MHz (not observable for the Ideal Chip loopback emission).

By comparison, the spectral content of the PCFM AWG waveforms and loopback emissions (Figs. 9 and 10) have far less distortion because the CPM structure, as evidenced by its widespread use in power and spectrally constrained communication applications [19-23], is amenable to the inherent spectral shaping and nonlinear nature of the transmitter (particularly the power amplifier). While the PCFM loopback emissions also experience some deviation in spectral content relative to their respective AWG

waveforms, this distortion only occurs below roughly −34 dB, thus inducing far less mismatch. Furthermore, the PCFM emissions possess noise-limited bandwidth of roughly 15 MHz, which is 60% of that demonstrated by the 10% Transition case, even though the necessary bandwidth (e.g. at −3 dB) is unchanged. As such, PCFM waveforms may serve as an enabler to address future requirements of spectral containment for high-power radar operation.
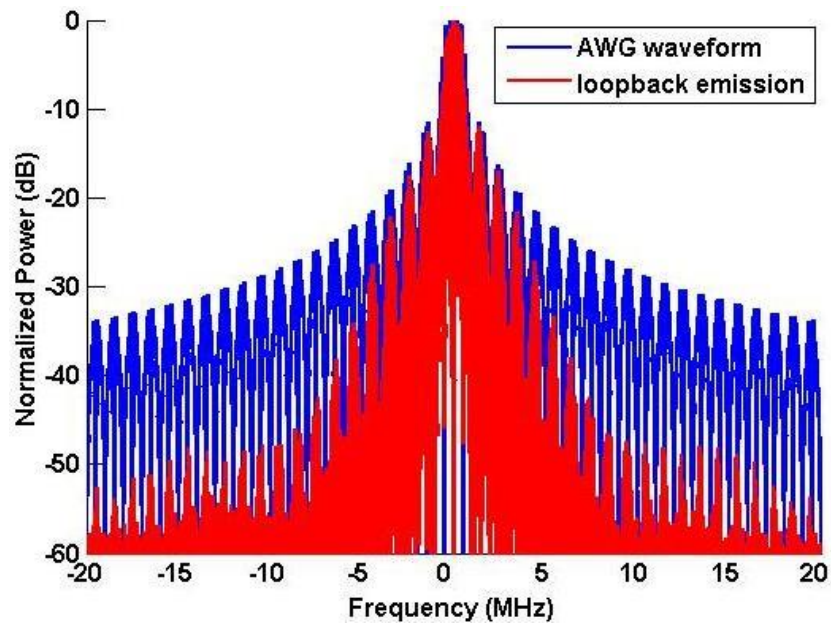

Figure 7: Spectral content of Ideal Chip waveform before and after the transmitter
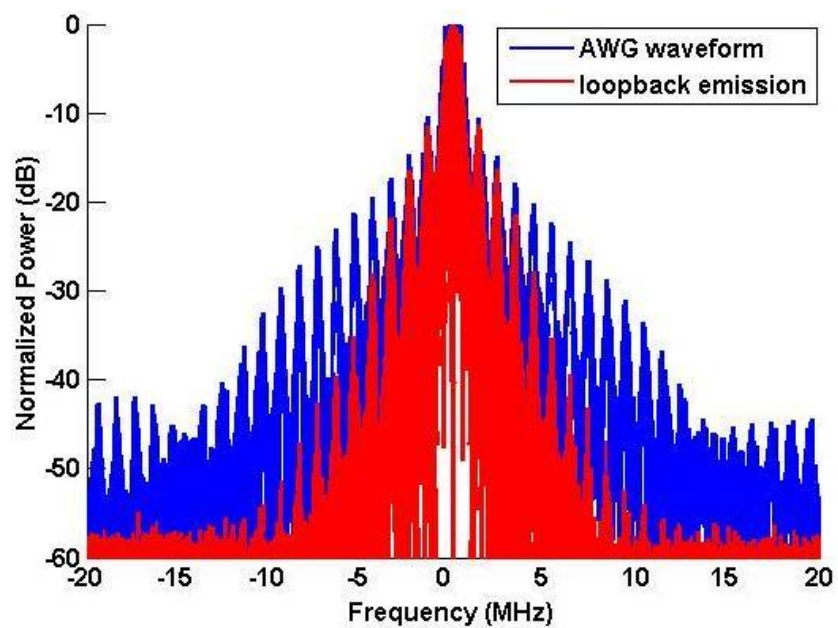
Figure 8: Spectral content of 10% Transition waveform before and after the transmitter
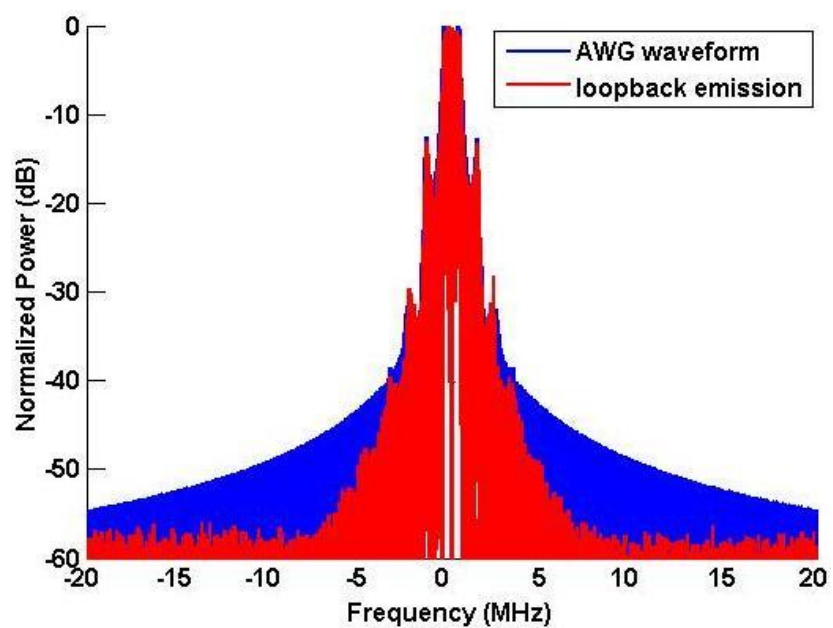
Figure 9: Spectral content of PCFM-RC waveform before and after the transmitter
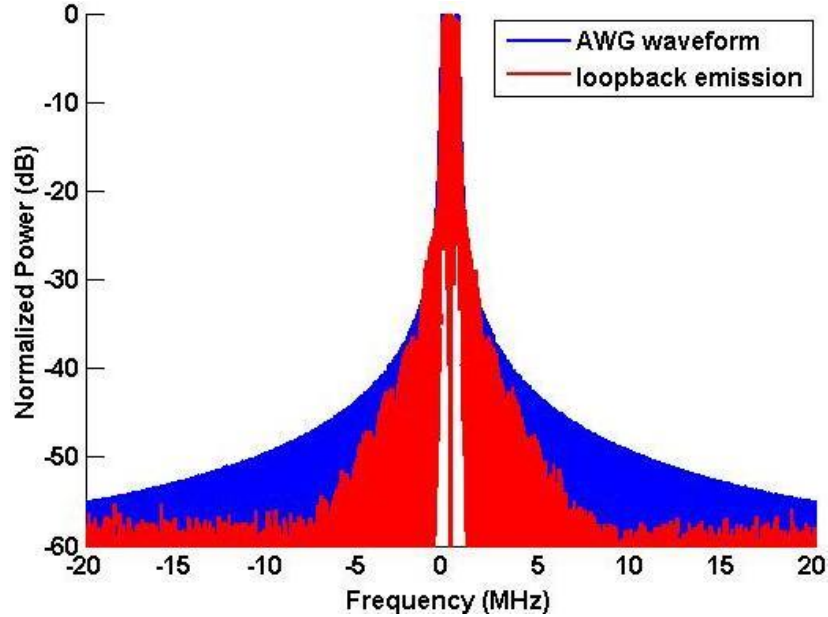
Figure 10: Spectral content of PCFM-RECT waveform before and after the transmitter

C) Receive Effects – Sampling and Mismatch

A pulsed emission cannot be truly bandlimited. The receiver sampling rate involves a trade-off in terms of data throughput / computational cost, noise rejection, and acceptable distortion from undersampling. To examine the four implementations with respect to receive sampling, the digitized AWG waveform and loopback emission, both of which consist of 150 samples per chip width, are lowpass filtered and downsampled. In accordance with the examination of straddling (cusping) loss in [12], here a Gaussian lowpass filter having a length of 4 chip widths and a cutoff frequency corresponding to the downsampling factor are used to decimate both the AWG waveform and loopback emission. We consider final sampling rates commensurate with $K = 1, 2, 3$, and 5 samples per chip width according to the definition in (4). Delay shifting the loopback emission prior to decimation permits the determination of straddling loss effects via (5) that are a result of mismatch from undersampling and transmitter distortion.

Figures 11 and 12 show the straddling loss with respect to delay $\tau \in [0, T_s]$ as a function of per-chip sampling factor K for the Ideal Chip and PCFM-RECT implementations, respectively. For both cases it is observed that $K = 1$ sample per chip yields the highest straddling loss, with PCFM-RECT being slightly worse at the maximum. As K increases to 2 and greater, however, it is clear that the PCFM waveform experiences a lower degree of loss. Noting that the Ideal Chip implementation never attains a true match (0 dB), these results may also be partially attributed to the distortion the Ideal Chip waveform encountered in the transmitter. As such, Figs. 11 and 12 can be considered to represent total mismatch from transmitter effects and receive sampling.

Using the straddling loss results in Figs. 11 and 12, as well as those for the 10% Transition and PCFM-RC waveforms (not shown), the maximum and mean straddling losses as a function of K are shown in Figs. 13 and 14, respectively. As expected, both figures reveal the straddling loss to decrease monotonically as K increases for all implementations, albeit with diminishing benefit. In Fig. 13 it is observed that, aside from $K = 1$, the CPM implementations yield a lower maximum loss than the idealized implementations. Likewise in Fig. 14 it is found that the CPM implementations have a lower measured mean loss for all values of K.
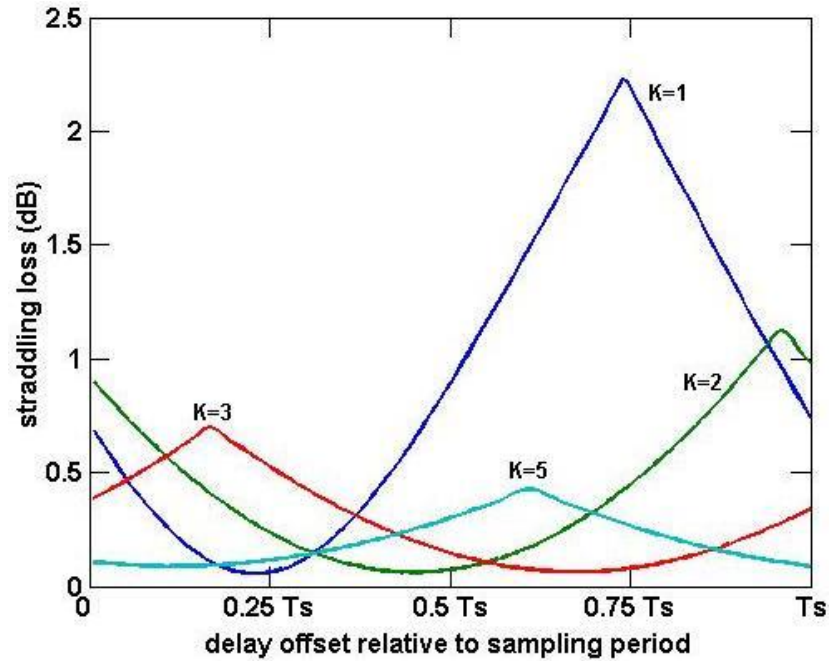
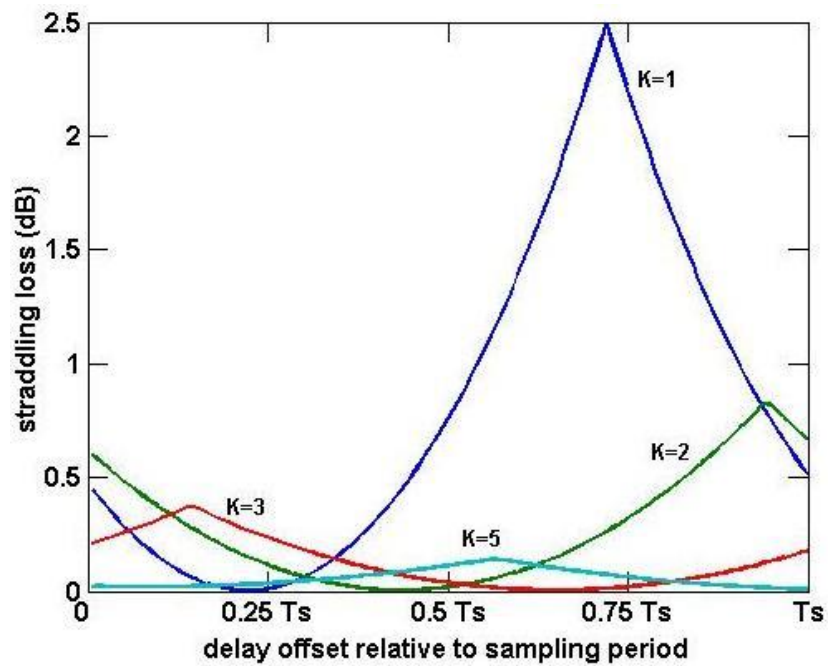**Figure 11: Straddling loss of Ideal Chip vs delay offset τ for *K* samples per chip width**

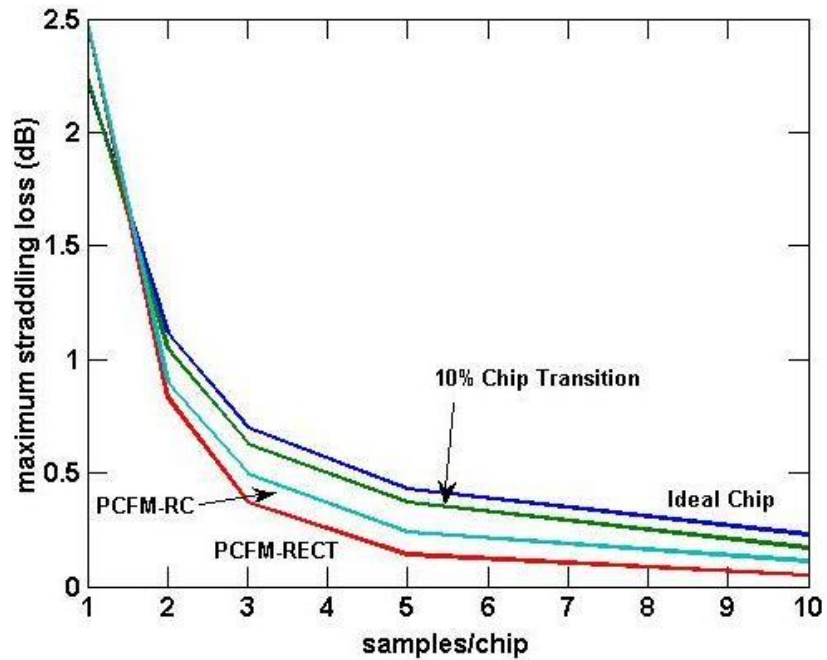**Figure 12: Straddling loss of PCFM-RECT vs delay offset τ for *K* samples per chip width**

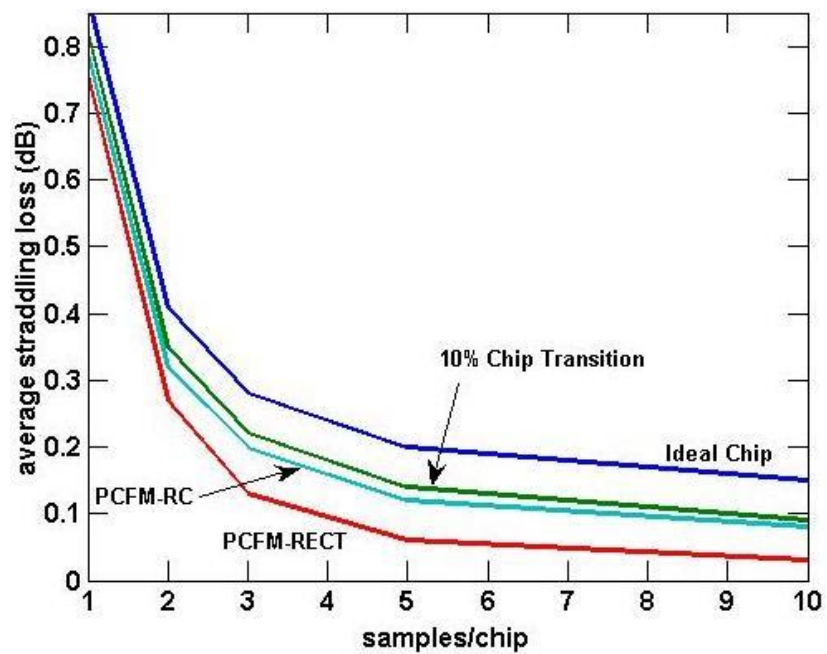**Figure 13:** **Maximum straddling loss over** $\tau \in \left[0, T_s \right]$ **vs sampling rate**

Figure 14: **Mean straddling loss over** $\tau \in \left[0, T_s \right]$ **vs sampling rate**

D) Receive Effects – Range Sidelobe Response

Using the versions of the AWG waveform and loopback emission decimated to $K = 5$ samples per chip interval, Figs. 15–18 reveal the resulting range correlations

where the AWG version is employed as a matched filter to the "point target reflection" of the decimated loopback emission. For the idealized waveform results in Figs. 15 and 16, the range sidelobes at the outermost delay offsets are observed to increase as one would expect from the use of the P4 code under idealized implementation [4]. In contrast, Fig. 17 shows the gradual range sidelobe roll-off that one expects from the LFM, which is closely approximated by the PCFM-RECT implementation of the P4 code. Note the slight ripple that occurs at the lower sidelobe values is due to the modest transmitter distortion of CPM. Finally, Fig. 18 illustrates the results for PCFM-RC, which is a blend of the LFM and P4 range sidelobe responses.
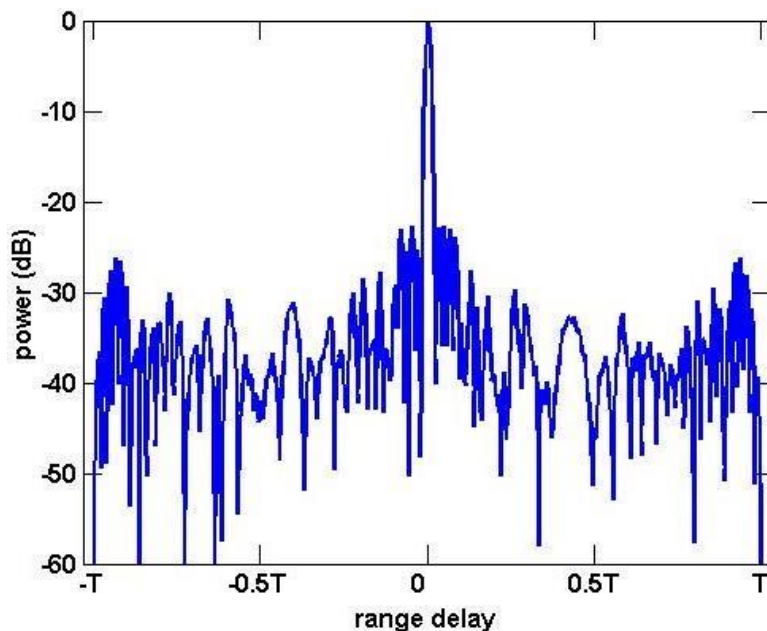

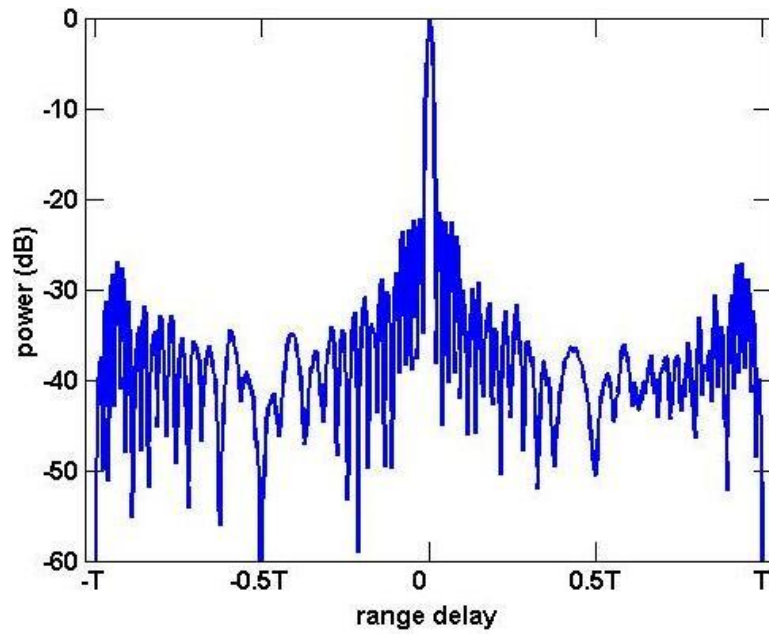**Figure 15: Matched filter response to loopback emission of Ideal Chip waveform**

Figure 16: Matched filter response to loopback emission of 10% Transition waveform
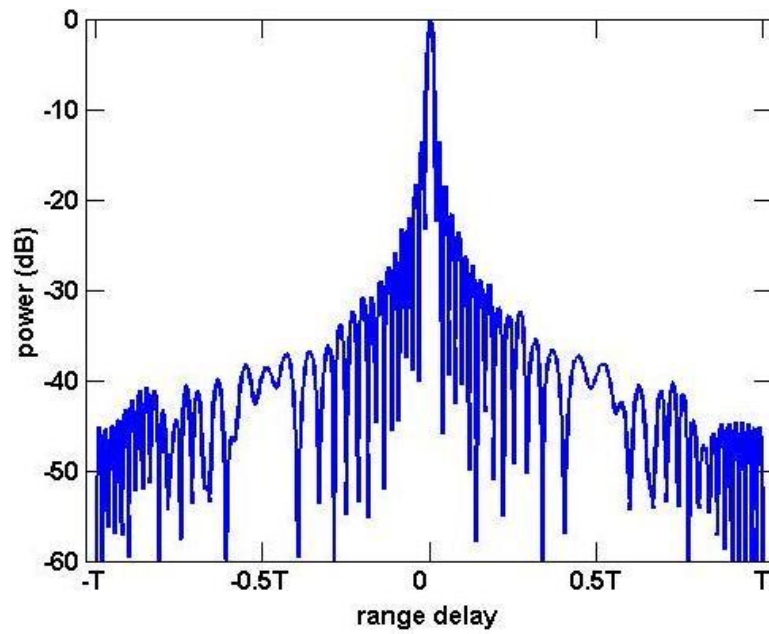

Figure 17: Matched filter response to loopback emission of PCFM-RECT waveform
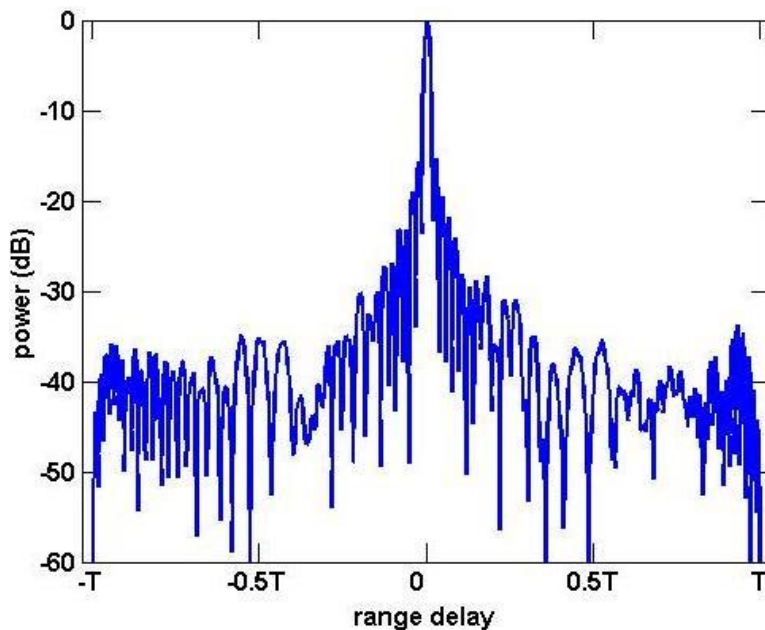
Figure 18: Matched filter response to loopback emission of PCFM-RC waveform

E) CPM Implementation of Previously Optimized Codes

Whereas the P4 code employed above represents a sampled version of an LFM, now a previously optimized code is considered which, when implemented using CPM, produces a nonlinear FM (NLFM) waveform for PCFM. Here a length-64 polyphase Barker code [28] is used. With the test setup described in [14] and 25 samples per chip width, followed by decimation using a 4 chip width Gaussian lowpass filter to $K = 5$ samples per chip width, the resulting decimated AWG waveform is used as the matched filter to the similarly decimated loopback emission. Figure 19 depicts the matched filter responses for the Ideal Chip and PCFM-RECT implementations (the results from the other two implementations are negligibly different). Of particular note is that in terms of peak sidelobe level (PSL), the criterion for which this code was optimized [28], the Ideal Chip implementation yields far better performance than the CPM-implemented waveform. It can thus be inferred that CPM, by introducing a deviation from the idealistic square chip structure upon which optimization was performed, results in some

degradation in the level of the range sidelobes, though the trade-off is that CPM facilitates the capability for actual implementation on a high-power radar.
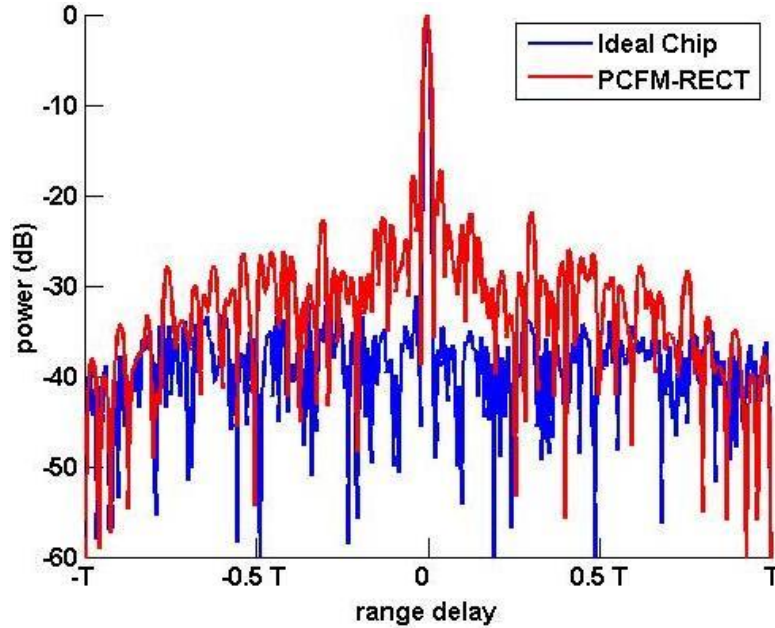

Figure 19: Matched filter responses for Ideal Chip and PCFM-RECT implementations of a 64-length polyphase Barker code

By applying the mismatch filter (MMF) formulation of Sect. III, Fig. 20 illustrates the MMF responses for the Ideal Chip and PCFM-RECT implementations. Here $\lceil K/2 \rceil = 3$ rows above and below the mth row are set to zero, the mismatch filter is $M = 3$ times longer than the waveform, and the MMF for each case is diagonally loaded so as to achieve an identical mismatch loss of 0.5 dB. Under the MMF formulation, one observes that both implementations realize PSL reductions of roughly 8 dB. Thus the MMF can be used to compensate somewhat for the increase in range sidelobes experienced by the CPM implementation due to deviation from the idealized optimization framework.

These results for an optimized code demonstrate the need to account for the code-to-waveform implementation within the optimization process. In so doing, by direct

extension one could also incorporate the spectral shaping and nonlinear aspects of the transmitter. In the companion paper [14], this new paradigm of optimizing the physical radar emissions is explored.
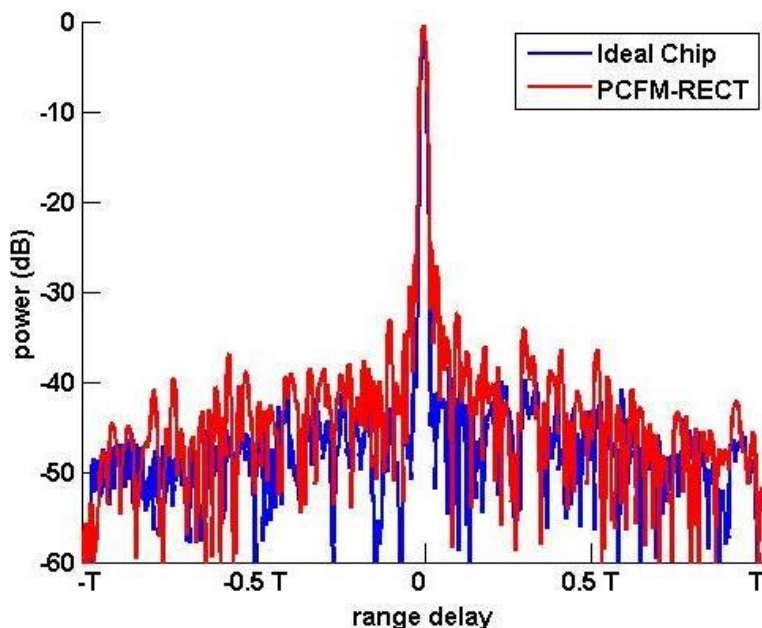

Figure 20: Mismatch filter responses for Ideal Chip and PCFM-RECT implementations of a 64-length polyphase Barker code

CONCLUSIONS

In this first paper of the two-part sequence, the continuous phase modulation (CPM) framework was modified for use as a means to implement radar codes as continuous polyphase-coded FM (PCFM) waveforms and ultimately as physical emissions. The new CPM scheme is amenable to the power and spectral efficiency goals of current and future radar systems that rely upon the operation of a saturated power amplifier to maximize power-added efficiency and associated distortion it induces. Furthermore, as is well-known for communication applications, CPM can be easily implemented in hardware using standard FM thus making it applicable to legacy radar systems as well without the need of an arbitrary waveform generator.

It was shown that the PCFM waveforms incur less distortion from the transmitter than traditional implementations of polyphase codes and, as a result, less mismatch loss on receive. It was also found that the waveforms produced by the CPM implementation of previously optimized codes experience some degradation in terms of range sidelobes with respect to the idealistic coded waveform (which possesses theoretically infinite bandwidth). For this reason, the companion paper addresses the notion of "transmitter-in-the-loop" optimization, whereby the code is determined according to the characteristics of the transmitter-distorted emission of the CPM-generated PCFM waveform.

REFERENCES

[1] S. Blunt, M. Cook, E. Perrins, and J. de Graaf, "CPM-based radar waveforms for efficiently bandlimiting a transmitted spectrum," *IEEE Radar Conf.*, Pasadena, CA, May 2009.

[2] R.H. Barker, "Group synchronization of binary digital systems," *Communication Theory*, Academic Press, London, pp. 273-287, 1953.

[3] B.L. Lewis and F.F. Kretschmer, "A new class of polyphase pulse compression codes and techniques," *IEEE Trans. AES*, vol. AES-17, no. 3, pp. 364-372, May 1981.

[4] B.L. Lewis and F.F. Kretschmer, "Linear frequency modulation derived polyphase pulse compression codes," *IEEE Trans. AES*, vol. AES-18, no. 5, pp. 637-641, Sept. 1982.

[5] G. Coxson and J. Russo, "Efficient exhaustive search for optimal-peak-sidelobe binary codes," *IEEE Trans. AES*, vol. 41, no. 1, pp. 302-308, Jan. 2005.

[6] N. Levanon and E. Mozeson, *Radar Signals*, John Wiley & Sons, Inc., Hoboken, NJ, 2004.

[7] J.D. Jenshak and J.M. Stiles, "A fast method for designing optimal transmit codes for radar," *IEEE Radar Conf.*, Rome, Italy, May 2008.

[8] C.J. Nunn and G.E. Coxson, "Polyphase pulse compression codes with optimal peak and integrated sidelobes," *IEEE Trans. AES*, vol. 45, no. 2, pp. 775-781, Apr. 2009.

[9] J. Li and P. Stoica, *MIMO Radar Signal Processing*, John Wiley & Sons, Inc., Hoboken, NJ, 2009.

[10] A. Nehorai, F. Gini, M.S. Greco, A.P. Suppappola, and M. Rangaswamy, Special Issue on "Adaptive waveform design for agile sensing and communication," *IEEE Journal of Selected Topics in Signal Processing*, vol. 1, no. 1, June 2007.

[11] W. Roberts, H. He, J. Li, and P. Stoica, "Probing waveform synthesis and receiver filter design," *IEEE Signal Processing Magazine*, vol. 27, no. 4, pp. 99-112, July 2010.

[12] A.M. Klein and M.T. Fujita, "Detection performance of hard-limited phase-coded signals," *IEEE Trans. AES*, vol. AES-15, no. 6, pp. 795-802, Nov. 1979.

[13] F.H. Raab, P. Asbeck, S. Cripps, P.B. Kenington, Z.B. Popovic, N. Pothecary, J.F. Sevic, and N.O. Sokal, "Power amplifiers and transmitters for RF and microwave," *IEEE Trans. Microwave Theory & Techniques*, vol. 50, no. 3, pp. 814-826, Mar. 2002.

[14] S.D. Blunt, J. Jakabosky, M. Cook, J. Stiles, S. Seguin, E.L. Mokole, "Polyphase-coded FM (PCFM) waveforms: part II: optimization," to appear in *IEEE Trans. AES*.

[15] H. Faust, B. Connolly, T.M. Firestone, R.C. Chen, B.H. Cantrell, and E.L. Mokole, "A spectrally clean transmitting system for solid state phased-array radars," *IEEE Radar Conf.*, Philadelphia, PA, pp. 140-144, Apr. 2004.

[16] J.W. Taylor and H.J. Blinchikoff, "Quadriphase code – a radar pulse compression signal with unique characteristics," *IEEE Trans. AES*, vol. 24, no. 2, pp. 156-170, Mar. 1988.

[17] R. Chen and B. Cantrell, "Highly bandlimited radar signals," *IEEE Radar Conf.*, Long Beach, CA, pp. 220-226, Apr. 2002.

[18] H. Griffiths, S. Blunt, L. Cohen, and L. Savy, "Challenge problems in spectrum engineering and waveform diversity," *IEEE Radar Conf.*, Ottawa, Canada, Apr./May 2013.

[19] J.B. Anderson, T. Aulin, and C.-E. Sundberg, *Digital Phase Modulation*, Plenum Press, New York, NY, 1986.

[20] *IRIG Standard 106-00: Telemetry Standards*, Range Commanders Council Telemetry Group, Range Commanders Council, White Sands Missile Range, New Mexico.

[21] E. Perrins and M. Rice, "Reduced complexity detectors for multi-h CPM in aeronautical telemetry," *IEEE Trans. AES*, vol. 43, no. 1, pp. 286-300, Jan. 2007.

[22] *Bandwidth-Efficient Modulations: Summary of Definitions, Implementation, and Performance*, Report Concerning Space Data System Standards, Informational Report CCSDS 413.0-G-2.

[23] *Specifications of the Bluetooth System*, Bluetooth Special Interest Group, ver. 1.2, Nov. 2003.

[24] M.A. Richards, J.A. Scheer, and W.A. Holm, *Principles of Modern Radar: Basic Principles*, SciTech Publishing, pp. 786-787, 2010.

[25] M.H. Ackroyd and F. Ghani, "Optimum mismatch filters for sidelobe suppression," *IEEE Trans. AES*, vol. AES-9, no. 2, pp. 214-218, Mar. 1973.

[26] S.D. Blunt, K. Gerlach, and T. Higgins, "Aspects of radar range super-resolution," *IEEE Radar Conf.*, Waltham, MA, pp. 683-687, Apr. 2007.

[27] S.D. Blunt, M.R. Cook, and J. Stiles, "Embedding information into radar emissions via waveform implementation," *Intl. Waveform Diversity and Design Conf.*, Niagara Falls, Canada, pp. 195-199, Aug. 2010.

[28] C. Nunn, "Constrained optimization applied to pulse compression codes and filters," *IEEE Intl. Radar Conf.*, Arlington, VA, pp. 190-194, May 2005.

[29] F.H. Sanders, R.L. Hinkle, and B.J. Ramsey, "Measurement procedures for the radar spectrum engineering criteria (RSEC)," *NTIA Report TR-05-420*, Mar. 2005.